CEAS-GNC-2024-018

EuroGNC Navigation Guidance Control CEAS Bristol, UK June 11th-13th 2024
University of BRISTOL ROYAL AERONAUTICAL SOCIETY AIAA

Control design for rendezvous operation near Halo Orbits using Lyapunov-Floquet theory and AUTO

Joaquin G. López-Cepero MSc Student, Universidad de Sevilla, Department of Applied Mathematics, 41092, Seville, Spain. joaquingonzalezlc00@gmail.com

Jorge Galan-Vioque Professor, Universidad de Sevilla, Department of Applied Mathematics, 41092, Seville, Spain. jgv@us.es

Rafael Vazquez Professor, Universidad de Sevilla, Department of Aerospace Engineering, 41092, Seville, Spain. rvazquez1@us.es

ABSTRACT

This work investigates the design of an impulsive controller for rendezvous operation near periodic Halo Orbits using the Lyapunov-Floquet theory. Using the Circular Restricted Three-Body Problem (CR3BP), a framework extensively discussed in the literature, a numerical continuation via AUTO 07P is employed to develop the bifurcation diagram for the H1 family of Halo orbits. Then, the Lyapunov-Floquet transformation enables the conversion of the periodic Linear Time Variant (LTV) system, derived from the linearization of the equations of motion, into an analytical solution which takes the form of an exponential for all time instances, thereby simplifying the design process for the controller. An impulsive control strategy is adopted for evaluating the performance of this approach, culminating in the development and testing of a simple LQR controller, to have an initial assessment of its efficacy compared with previous approaches.

Keywords: Spacecraft rendezvous; Halo orbits; Floquet theory; LQR

Nomenclature

$\mathbf{\Phi}(t_0, \mathbf{x}_0; t_1)$	=	State transition matrix from $t_0, \mathbf{x}_0$ to $t = t_1$
$\mathbf{x}_t(t)$	=	Absolute state of the target
$\mathbf{r}_t(t)$	=	Absolute position of the target
$\mathbf{v}_t(t)$	=	Absolute velocity of the target
$\hat{\mathbf{x}}(t)$	=	Absolute state of the chaser
$\hat{\mathbf{r}}_t(t)$	=	Absolute position of the chaser
$\hat{\mathbf{v}}_t(t)$	=	Absolute velocity of the chaser
$\mathbf{x}(t)$	=	Relative state of the chaser with respect to the target
μ	=	Parameter of the masses in the C3RBP
T	=	Period of closed orbit
λ	=	Continuation parameter in the CR3BP
$\mathbf{L}_{2T}$	=	Lyapunov-Floquet change of basis matrix.
$\mathbf{A}_k$	=	State matrix of the linearized system
$\hat{\mathbf{A}}_k$	=	Transformed state matrix

B = Input matrix
K = Control gain

1 Introduction

The exploration of multi-body environments, particularly in the context of space missions, has emerged as an increasingly active area of research. This surge in interest is partially fueled by the International Space Station (ISS) partners' ambitions to establish a space station in cislunar space, known as the Lunar Gateway (or just Gateway) [1]. The strategic placement of the Gateway in lunar orbit promises to significantly enhance scientific exploration by enabling exploration of the Solar System or e.g. facilitating the return of lunar samples [2].

Studies exploring various orbital locations for the Gateway have identified Near Rectilinear Halo Orbits (NRHOs) around the Earth-Moon L_2 point as particularly viable, owing to their favorable stability properties and persistence in more accurate models [3, 4]. These orbits are part of the larger family of Halo orbits in the Circular Restricted Three-Body Problem (CR3BP), a framework extensively discussed in the literature [5].

Far-rendezvous operations, driven primarily by fuel efficiency, have been well-explored. For example, by exploiting properties of the stable and unstable manifolds [6]. Reference [7] compares the fuel efficiency of invariant manifolds connections with that of classical phasing strategies. Additionally, a surrogate-based parameter optimization strategy is employed in [8] to tackle the problem.

On the other hand, the field of close rendezvous operations, is now gaining attraction. In particular, a proposal for the definition of the relative motion equations in the LVLH frame for rendezvous in lunar orbits is given by [9], which is interesting for rendezvous operations as pointed out in [10]. Additionally, rendezvous scenarios around L2 halo orbits for future transportation missions have been studied on [11], and [12] discusses the rendezvous targeting and navigation by applying a navigation filter. Moreover, [13] discusses different linear and non-linear models used to describe cis-lunar relative motion, with special focus on NRHO. Recent works on rendezvous have also explored optimization with uncertainty management [14–16] and those have also been translated into the context of CR3BP [17, 18].

However, how to describe and solve linearized relative dynamics close to Halo orbits is still unclear, compared with the fully established theories for relative dynamics in the two-body problem. In this context, this work investigates in particular the application of the Lyapunov-Floquet change of variables [19] in designing a controller for the rendezvous challenge on a Halo orbit in the Earth-Moon system. Using the Circular Restricted Three Body Problem (CR3BP) model (described in Section 2), with a focus on the H1 family of orbits, we employ numerical continuation via AUTO 07P to develop the bifurcation diagram for the CR3BP, as explained in Section 3.

The subsequent computation of the Lyapunov-Floquet transformation for a specific orbit facilitates the conversion of the periodic Linear Time Variant (LTV) system, derived from the linearization of the motion equations, into a Linear Time Invariant (LTI) system. This transformation enables the derivation of an analytical solution which takes the form of an exponential for all time instances, thereby simplifying the design process for the controller. An impulsive control strategy is adopted for evaluating the performance of this innovative approach, culminating in the development and testing of a simple LQR controller, given in Section 4 to have an initial assessment of its efficacy.

The main contribution of this work is the comparison between using the proposed transformation to compute the control law or directly discretizing the CR3BP equations, as given in Section 5 together with a simulation study of the proposed controller. The paper is closed with some concluding remarks in Section 6.

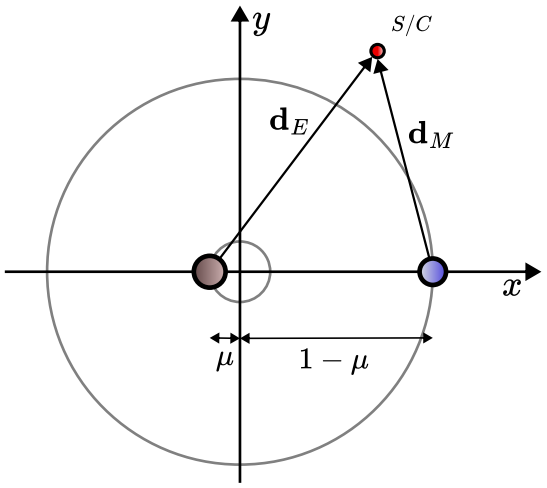

Fig. 1 Schematic representation of the CR3BP in the synodic reference frame

2 The circular restricted three body problem

The CR3BP is a specific case of the three-body problem (the scenario considering the dynamics of three massive bodies subject to their mutual gravitational attraction). The main assumptions are: the mass of the primaries is much greater than the mass of the third body and thus the latter is neglected; the primaries follow circular orbits around the center of mass of the system; a synodic frame of reference is usually used to express the equations. This frame of reference is defined with a certain angular speed $\omega = [0, 0, \omega_z]^T$ such that both primaries always lie on the X-axis.

In order to non-dimensionalize the equations, the following reference quantities are defined:

$$m^* = m_1 + m_2, \quad d^* = |\mathbf{r}_1 - \mathbf{r}_2|, \quad t^* = 1/\omega_z, \tag{1}$$

where m_1, m_2 are the masses of both primaries and $\mathbf{r}_1$ and $\mathbf{r}_2$ are their position vector.

A characteristic parameter μ is used to describe the system. This parameter is defined as:

$$\mu = \frac{m_2}{m_1 + m_2}. \tag{2}$$

In the particular case of the Earth-Moon system: $\mu \simeq 1.215058 \times 10^{-2}$.

2.1 Equations of motion (non-dimensionalized)

Defining the state $\mathbf{x} = (x, y, z, \dot{x}, \dot{y}, \dot{z})$, the equations that describe the CR3BP are the following, once they have been nondimensionalized using the aforementioned reference values

$$\dot{\mathbf{x}} = \mathbf{f}(\mathbf{x}) = \begin{pmatrix} \dot{x} \\ \dot{y} \\ \dot{z} \\ 2\dot{y} + x - (1-\mu)\dfrac{x+\mu}{d_E^3} - \mu\dfrac{x-1+\mu}{d_M^3} \\ -2\dot{x} + y - (1-\mu)\dfrac{y}{d_E^3} - \mu\dfrac{y}{d_M^3} \\ -(1-\mu)\dfrac{z}{d_E^3} - \mu\dfrac{z}{d_M^3} \end{pmatrix} \tag{3}$$

where $d_E = \sqrt{(x+\mu)^2 + y^2 + z^2}$ and $d_M = \sqrt{(x+\mu-1)^2 + y^2 + z^2}$.

3 Numerical Continuation: AUTO

The aim of this section is to describe the procedure by which the Halo Orbit family is computed using the software AUTO [20].

Given a general problem $\dot{\mathbf{u}} = \mathbf{h}(\mathbf{u}, \lambda)$, that depends on a parameter $\lambda \in \mathbb{R}$ and the state vector $\mathbf{u} \in \mathbb{R}^n$. Finding a solution for this equation is equivalent to finding a solution to

$$\mathbf{H}(\mathbf{z}) = \dot{\mathbf{u}} - \mathbf{h}(\mathbf{z}) = \mathbf{0}, \quad \mathbf{z} = (\mathbf{u}, \lambda) \in \mathbb{R}^{n+1} \tag{4}$$

A given solution continues to be regular (i.e. exists locally as a unique unidimensional family of solutions [21]) when the $n \times n + 1$ matrix, $\mathbf{H_z} = \partial\mathbf{H}/\partial\mathbf{z}$, has maximum rank.

When this condition is not fulfilled, the requirements of the Implicit Function Theorem are not satisfied, and a singular point is found. In these points, it is not possible to ensure that the solution is unique. The branching points in the bifurcation diagram are singular points [21]. AUTO uses Keller's pseudoarclength continuation method to obtain solution families from a certain initial solution $\mathbf{z}_0 = (\mathbf{x}_0, \lambda_0)$. In order to compute the periodic solutions, AUTO solves the following BVP:

$$\dot{\mathbf{u}} = T\mathbf{f}(\mathbf{u}, \lambda), \quad \mathbf{u}, \mathbf{f} \in \mathbb{R}^n, \lambda, T \in \mathbb{R} \tag{5}$$

$$\mathbf{u}(0) = \mathbf{u}(1) \tag{6}$$

where the period T, and λ are used as continuation parametres. Furthermore, an adequate phase condition is used (e.g. *Poincaré orthogonality condition* or the *integral phase condition*, deduced in [22]).

3.1 Periodic orbits in conservative systems: unfolding parameter

In the case of conservative systems (such as that of the CR3BP), one option for continuing solutions is artificially increasing the dimension of the system by adding a "damping" term, that is normally called "*unfolding parameter*". As a consequence, the system that AUTO works with is a modified version of (3) as follows

$$\dot{\mathbf{x}} = \begin{pmatrix} \dot{x} \\ \dot{y} \\ \dot{z} \\ 2\dot{y} + x - (1-\mu)\dfrac{x+\mu}{d_E^3} - \mu\dfrac{x-1+\mu}{d_M^3} + \lambda x_4 \\ -2\dot{x} + y - (1-\mu)\dfrac{y}{d_E^3} - \mu\dfrac{y}{d_M^3} + \lambda x_5 \\ -(1-\mu)\dfrac{z}{d_E^3} - \mu\dfrac{z}{d_M^3} + \lambda x_6 \end{pmatrix} \tag{7}$$

where λ is the unfolding parameter.

As λ is a damping term, it is not possible to find periodic solutions if $\lambda \neq 0$. In this way, the periodicity of the solution requires $\lambda \simeq 0$ (down to numerical precision).

3.2 Obtained solutions: H1 family

The Halo H1 family of orbits emerges from the family of planar Lyapunov orbits as a bifurcation with a nonzero vertical component. Refer to [5] for a detailed analysis on the characteristics of this family of orbits.

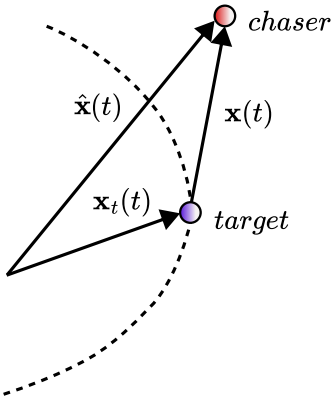

Fig. 3 Schematic representation of $\mathbf{x}(t)$ in state space.

The bifurcation diagram corresponding to the H1 family is shown in Figure 2a. Additionally, Figure 2b show the set of periodic solutions found during the numerical propagation. Some of these orbits will be used to analyze the control strategy.

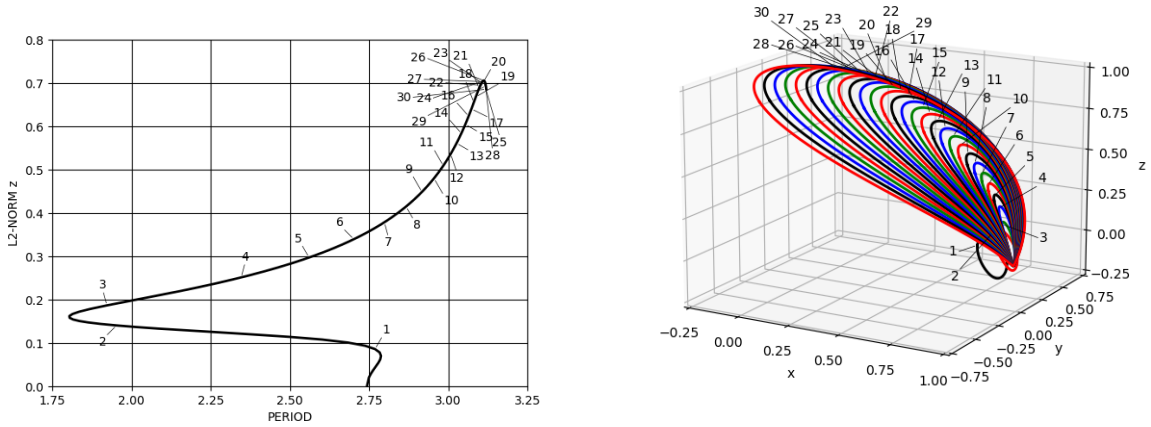

(a) Bifurcation diagram obtained with AUTO. **(b) Periodic orbits from the H1-Family obtained by numerical continuation on AUTO.**

Fig. 2 Results obtained by numerical continuation of periodic orbits from the H1 family with AUTO

3.3 Variational equations describing the relative motion

Let $\mathbf{x}_t(t)$ be a periodic solution of system (3) used as the reference, which may describe the motion of the target around the halo orbit. Let the chaser's state vector be described by $\hat{\mathbf{x}} = \mathbf{x} + \mathbf{x}_t(t)$, where $\mathbf{x}_t(t)$ is the relative state. Schematically, Figure 3 shows this setup.

Developing the dynamics of the chaser $\mathbf{f}(\hat{\mathbf{x}}) = \mathbf{f}(\mathbf{x}(t) + \mathbf{x}_t(t))$ around the target's position at a certain time instant t:

$$\dot{\mathbf{x}}(t) + \dot{\mathbf{x}}_t(t)) = \mathbf{f}(\mathbf{x}(t)) + \mathbf{x}_t(t)) = \mathbf{f}(\mathbf{x}_t(t)) + \nabla\mathbf{f}(\mathbf{x}_t(t))\mathbf{x}(t) + \mathbf{h}(\mathbf{x}_t(t), \mathbf{x}(t)) \tag{8}$$

Using (3) and discarding higher-order terms:

$$\dot{\mathbf{x}}(t) = \mathbf{A}(t)\mathbf{x}(t), \tag{9}$$

where $\mathbf{A}(t) = \nabla\mathbf{f}(\mathbf{x}_t(t))\mathbf{x}(t)$.

3.4 Lyapunov-Floquet change of variables

In this section, a general description of the Lyapunov-Floquet change of variables is given. For a more in-depth analysis, refer to [19], [23], [24]. Given a Linear Time Periodic (LTP) system of the type:

$$\dot{\mathbf{x}} = \mathbf{A}(t)\mathbf{x}, \tag{10}$$

where $\mathbf{A}(t)$ is a continuous periodic function of period T, $\mathbf{x}(t) \in \mathbb{R}^n$ and $t \in \mathbb{R}$. Let $\mathbf{\Phi}(t; t_0)$ be the state transition matrix (STM) of the system (10) from t_0 to t. $\mathbf{\Phi}(t; t_0)$ is continuous and has continuous derivative and $|\mathbf{\Phi}(t; t_0)| \geq 0$. From now on, without losing generality, $t_0 = 0$ and $\mathbf{\Phi}(t; 0) = \mathbf{\Phi}(t)$. $\mathbf{\Phi}$ satisfies

$$\mathbf{\Phi}(t + T) = \mathbf{\Phi}(t)\mathbf{\Phi}(T) \quad \forall t. \tag{11}$$

Since $\mathbf{\Phi}(T)$ is nonsingular, it is possible to define $\mathbf{F} \in \mathbb{C}^{nxn}$ such that

$$\mathbf{\Phi}(T) = e^{\mathbf{F}T} \tag{12}$$

For each matrix $\mathbf{F}$ that satisfies (12), there exists a periodic function of period T, $\mathbf{L}(t)$, such that

$$\mathbf{\Phi}(t) = \mathbf{L}(t)e^{t\mathbf{F}} \tag{13}$$

Additionally, it can be shown that taking

$$\mathbf{\Phi}(T)^2 = \mathbf{\Phi}(T)\mathbf{\Phi}(T) = e^{2T\mathbf{F}_{2T}} \tag{14}$$

there exist a periodic function of period T, $\mathbf{L}_{2T}(t)$, and a real matrix $\mathbf{F}_{2T} \in \mathbb{R}^{nxn}$ [23] such that

$$\mathbf{\Phi}(t) = \mathbf{L}_{2T}(t)e^{t\mathbf{F}_{2T}}. \tag{15}$$

The latter result is the one used in this project due to the obvious advantages that imply having a real matrix of coefficients in the transformed system.

The following time-dependent change of variables is defined:

$$\mathbf{x}(t) = \mathbf{L}_{2T}(t)\mathbf{z}(t) \tag{16}$$

Introducing the transformation in (10):

$$\dot{\mathbf{L}}_{2T}(t)\mathbf{z}(t) + \mathbf{L}_{2T}(t)\dot{\mathbf{z}}(t) = \mathbf{A}(t)\mathbf{L}_{2T}(t)\mathbf{z}(t) \tag{17}$$

Since $\mathbf{\Phi}(t)$ satisfies (23),

$$\dot{\mathbf{L}}_{2T}(t)e^{t\mathbf{F}_{2T}} + \mathbf{L}_{2T}(t)\mathbf{F}_{2T}e^{t\mathbf{F}_{2T}} = \mathbf{A}(t)\mathbf{L}_{2T}(t)e^{t\mathbf{F}_{2T}} \Rightarrow \dot{\mathbf{L}}_{2T}(t) + \mathbf{L}_{2T}(t)\mathbf{F}_{2T} = \mathbf{A}(t)\mathbf{L}_{2T}(t) \tag{18}$$

Introducing (18) in (17):

$$\dot{\mathbf{z}}(t) = \mathbf{F}_{2T}\mathbf{z}(t), \tag{19}$$

that is a Linear Time Invariant (LTI) system (i.e. it does not explicitly depend on time t) in the newly base defined by $\mathbf{L}_{2T}(t)$.

4 Impulsive control in the C3RBP

We now consider the model (3) with impulsive control, this is, the velocity can be instantaneously changed after a time Δt. Based on (19), it is possible to obtain an analytic solution of the form

$$\mathbf{z}(t) = e^{\mathbf{F}_{2T}(t-t_0)}\mathbf{z}(t_0) \tag{20}$$

where $\mathbf{z}(t_0)$ is the initial condition.

Taking N equidistant time instants such that $t_k - t_{k-1} = \Delta t$:

$$\mathbf{z}_{k+1} = e^{\mathbf{F}_{2T}\Delta t}\mathbf{z}(t_k) \tag{21}$$

Reverting the change of variables given by $\mathbf{L}_{2T}$ and introducing the impulsive control $\mathbf{u}_k$ in the instant t_k

$$\mathbf{x}_{k+1} = \mathbf{L}_{2T}(t_{k+1})e^{F_{2T}\Delta t}\mathbf{L}_{2T}^{-1}(t_k)\mathbf{x}(t_k) + \mathbf{B}\mathbf{u}_k \Rightarrow \mathbf{x}_{k+1} = \hat{\mathbf{A}}_k\mathbf{x}_k + \mathbf{B}\mathbf{u}_k \quad k = 1\ldots N-1 \tag{22}$$

where $\mathbf{B} = [\mathbf{0}, \mathbf{I}_3]^T$, and $\mathbf{u}_k \in \mathbb{R}^3$.

To obtain the matrices $\hat{\mathbf{A}}_k$, it is necessary to integrate numerically the IVP that defines the STM:

$$\dot{\mathbf{\Phi}}(t;0) = \mathbf{A}(t)\mathbf{\Phi}(t;0), \quad \mathbf{\Phi}(t_0;0) = \mathbf{I}_n \tag{23}$$

together with the system (10).

4.1 Linear Quadratic Regulator (LQR) design

In this section, the control problem is solved by using a discrete-time LQR. These controllers solve the following problem:

$$\min_{\mathbf{u}} J = \mathbf{x}_N^T\mathbf{Q}_N\mathbf{x}_N + \sum_{k=1}^{k=N-1}\mathbf{x}_k^T\mathbf{Q}_k\mathbf{x} + \mathbf{u}_k^T\mathbf{R}\mathbf{u}_k \tag{24}$$

computing iteratively the matrix $\mathbf{P}_k$ backwards in time from time instant $t_{k=N}$ to $t_{k=1}$:

$$\mathbf{P}_{k-1} = \hat{\mathbf{A}}_k^T P_k\hat{\mathbf{A}}_k - \hat{\mathbf{A}}_k^T\mathbf{P}_k\mathbf{B}_k(\mathbf{R}_k + \mathbf{B}_k^T\mathbf{P}_k\mathbf{B}_k)^{-1}\mathbf{B}_k^T\mathbf{P}_k\hat{\mathbf{A}}_k + \mathbf{Q}_k \tag{25}$$

with the initial condition $\mathbf{P}_N = \mathbf{Q}_N$, given by the terminal cost. In the analyzed problem, $\mathbf{B}_k = [\mathbf{0}, \mathbf{I}_3]^T$. The control law is defined as

$$\mathbf{u}_k = -\mathbf{K}_k\mathbf{x}_k \tag{26}$$

where

$$\mathbf{K}_k = (\mathbf{R}_k + \mathbf{B}_k^T\mathbf{P}_{k+1}\mathbf{B}_k)^{-1}(\mathbf{B}_k^T\mathbf{P}_{k+1}\hat{\mathbf{A}}_k) \tag{27}$$

Since matrix $\hat{\mathbf{A}}_k$ is $2T$-periodic, it is necessary to solve the problem in the interval $[0, 2T]$. The control problem is completely defined for time instants $t_k > 2T$. [1]

5 Results

In this section, the results for the implemented control law (using the transformation) are discussed, first analyzing the worthiness of the transformation.

[1] Other alternative is to choose *quasi-T-periodic Floquet factorizations*, as described in [23] for reducing the computation interval to the original period $[0, T]$, increasing the computational efficiency.

Three periodic orbits of the H1 family are studied. From the whole set of orbits computed using AUTO, these orbits are selected in order to test the controller in a range of values of the non-dimensional period, which is directly related with the shape and dimensions of the orbit. The non-dimensional periods can be found in Table 1. Additionally, Figures 4-5 represent the chosen orbits.

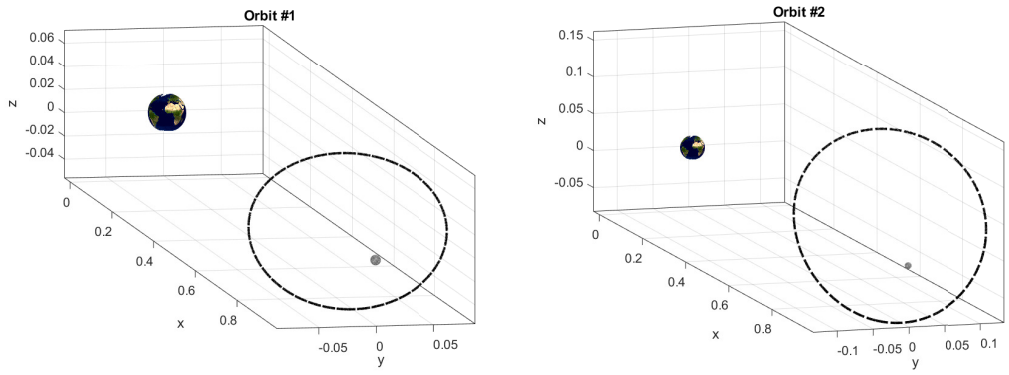

(a) Orbit #1 **(b) Orbit #2**

Fig. 4 Orbits # 1 y #2 in the Earth-Moon system.

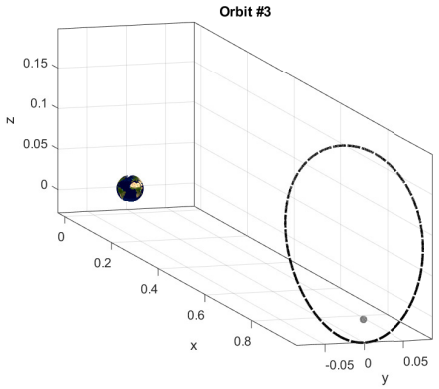

Fig. 5 Orbit #3 in the Earth-Moon system.

Table 1 Non-dimensional and dimensional periods of the chosen orbits.

Orbit #	1	2	3
$T[-]$	2.7718	2.6835	1.9530
T_{dim} [h]	290.74	281.48	204.86

5.1 Effect of the transformation on the LQR design

First, a brief comparison on the performance of the LQR design is given between a controller designed for the system untransformed states:

$$\mathbf{x}_{k+1} = \hat{\mathbf{A}}_k \mathbf{x}_k + \mathbf{B}\mathbf{u}_k \quad k = 1 \ldots N-1 \tag{28}$$

and for the transformed states:

$$\mathbf{z}_{k+1} = e^{\mathbf{F}_{2T}\Delta t}\mathbf{z}_k + \mathbf{L}_{2T}^{-1}(t_{k+1})\mathbf{B}\mathbf{u}_k = \mathbf{A}^{(z)}\mathbf{z}_k + \mathbf{B}_k^{(z)}\mathbf{u}_k \tag{29}$$

Table 2 Comparison of the results for the controller design on each of the bases.

Case	$\bar{x}(2T)[m]$	$\bar{y}(2T)[m]$	$\bar{z}(2T)[m]$	$\dot{\bar{x}}(2T)[m/s]$	$\dot{\bar{y}}(2T)[m/s]$	$\dot{\bar{z}}(2T)[m/s]$	$\Delta V[m/s]$
$\mathbf{z}(t)$	-1704.215	172.704	-830.180	-3.766E-3	1.772E-3	3.339E-3	46.759
$\mathbf{x}(t)$	14.010	19.410	-20.672	87.735E-6	-184.618E-6	-99.050E-6	56.229

where $\mathbf{B} = [\mathbf{0}, \mathbf{I}_3]^T$, and $\mathbf{u}_k \in \mathbb{R}^3$ for both cases. Additionally, superindex (z) indicates that it corresponds to the transformed variables equation. The difference between both systems is which of the matrices is constant and which one is time-dependent. In $\mathbf{z}$, matrix $\mathbf{B}^{(z)}$ is time-dependent while the state matrix $\mathbf{A}$ is constant. On the other hand, the system in $\mathbf{x}$ coordinates has a state matrix that is time-dependent while having $\mathbf{B}$ constant.

For the wieght matrices, those collected in (30) were taken with $N = 50$.

$$\mathbf{Q}_k = \mathbf{I}_6, \quad \mathbf{R}_k = \mathbf{I}_3, \quad k = 1 \dots N-1, \quad \mathbf{Q}_N = 10^8 \mathbf{I}_6. \tag{30}$$

The initial relative state was

$$\mathbf{x}(0) = \mathbf{z}(0) = [10^{-2}, 10^{-2}, 0, 0, 0, 0]^T,$$

corresponding to 5436.2 km of initial separation. The initial conditions chosen for the target's position are:

$$\mathbf{x}_t(0) = [0.8474,\ -0.0798,\ 0.1137,\ -0.0704,\ 0.1947,\ 0.1337]^T, \tag{31}$$

which corresponds to an intermediate case between apolune and perilune.

Table 2 shows the final state in SI units for both controllers after simulating with the full nonlinear dynamics. It can be seen that the control $\mathbf{z}$ performs worse in comparison with its counterpart in terms of final error after two full periods. However, the error stays below 2 km for both cases. Additionally, it can be seen that the control cost is 20% larger when designing the controller in $\mathbf{x}$ with respect to the case of $\mathbf{z}$.

Figures 6 and 7 show the evolution of the figures of merit during the simulation. It can be seen that the control on $\mathbf{z}$ does not experience the oscillations that the alternative shows on the z coordinate where it overshoots above 5000 km from a zero initial value.

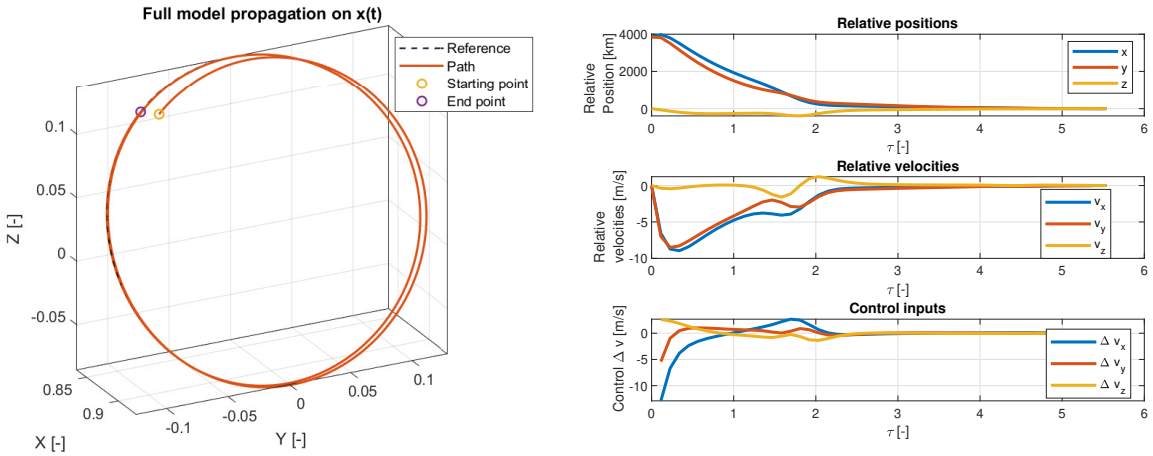

(a) Controlled trajectory **(b) State and control evolution**

Fig. 6 Simulation of the closed loop system performing the control on $\mathbf{x}(t)$.

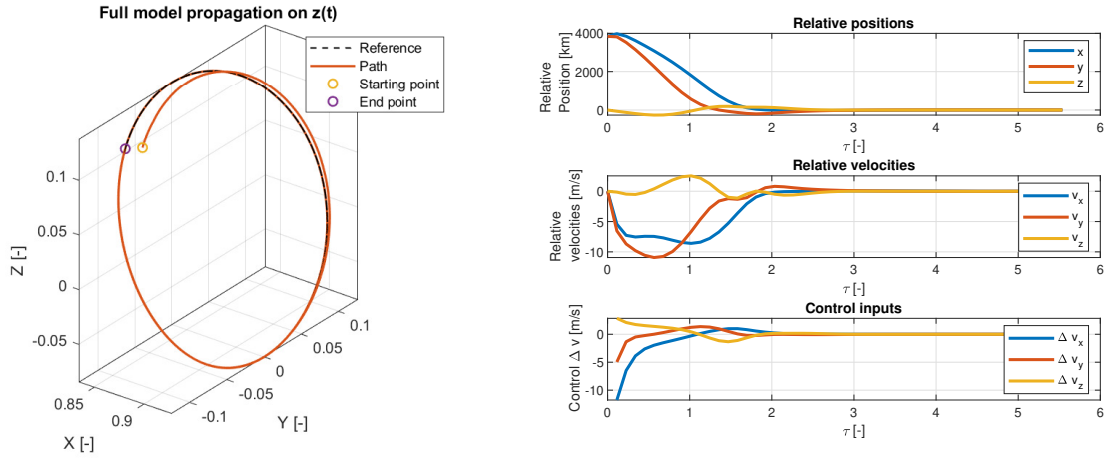

(a) Controlled trajectory **(b) State and control evolution**

Fig. 7 Simulation of the closed loop system performing the control on $\mathbf{z}(t)$.

5.2 Simulation results with the transformation

In this section, different cases are analyzed using the LQR model described in Section 4.1. As design parameters, those described in (32) were taken, with $N = 50$.

$$\mathbf{Q}_k = \mathbf{I}_6, \quad \mathbf{R}_k = 10^4\mathbf{I}_3, \quad k = 1 \dots N-1, \quad \mathbf{Q}_N = 10^9\mathbf{I}_6. \tag{32}$$

For each orbit, two cases are considered: one where the target is near the apolune at initial time and another where the target is near the perilune. The initial conditions of the target's state vector, $\mathbf{x}_t(0)$, are found in table 3.

Table 3 Initial conditions for the target's state vector, $\mathbf{x}_t(0)$, in the problem (3) for all the considered cases.

Orbit #	Case	$x_t(0)[-]$	$y_t(0)[-]$	$z_t(0)[-]$	$\dot{x}_t(0)[-]$	$\dot{y}_t(0)[-]$	$\dot{z}_t(0)[-]$
1	Apolune	0.8256	0.0105	0.0708	0.0086	0.1823	-0.0156
	Perilune	0.8775	-0.0075	-0.056	-0.0033	-0.2162	0.015
2	Apolune	0.8472	0.0521	0.1526	0.0504	0.2429	-0.0867
	Perilune	0.9537	-0.0316	-0.0787	-0.0291	-0.4204	0.105
3	Apolune	0.9885	-0.031	-0.019	-0.0935	-0.6647	0.4062
	Perilune	0.8979	-0.02	0.1962	-0.0282	0.1874	0.0497

The initial conditions for the relative state of the chaser with respect to the target, $\mathbf{x}(0)$, are given by

$$\mathbf{x}(0) = [10^{-2}, 10^{-2}, 0, 0, 0, 0]^T,$$

which corresponds to 5436.2 km of initial separation. Figures 8 - 13 show the results of the closed-loop simulations. For these simulations, the full non-linear dynamics (3) are used.

Table 4 contains the final relative states of the chaser with respect to the target after two full periods of simulation, $\bar{\mathbf{x}}(2T)$ and the total control cost ΔV_{total}. As can be seen, the final state is reduced to a few meters after two full periods. Additionally, as expected, apolune cases imply a lower cost in ΔV as well as a better controller behavior. Finally, as the period of the orbits is reduced, these tend to be more eccentric, increasing the differences between the apolune and perilune cases for the controller performance.

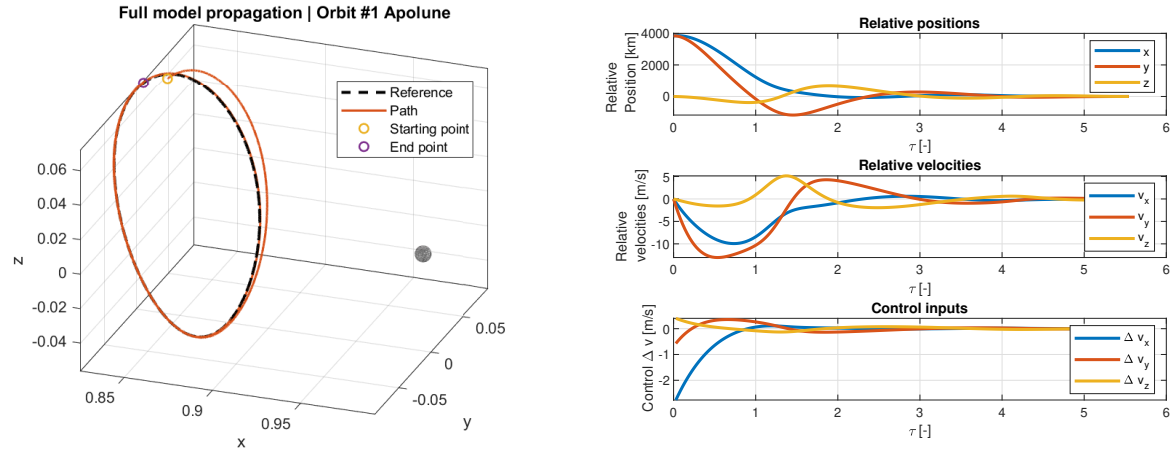

(a) Controlled trajectory **(b) State and control evolution**

Fig. 8 Simulation of the closed loop system for orbit #1 (apolune case).

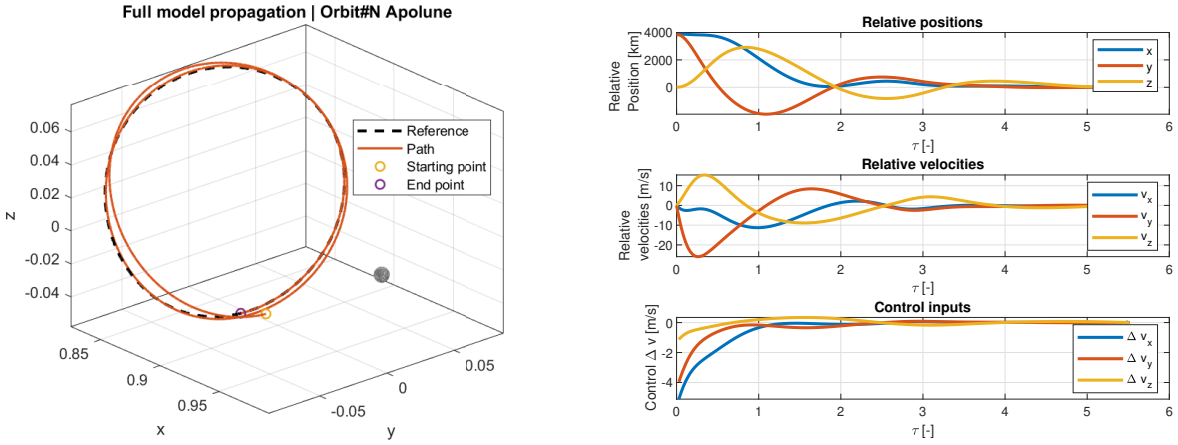

(a) Controlled trajectory **(b) State and control evolution**

Fig. 9 Simulation of the closed loop system for orbit #1 (perilune case).

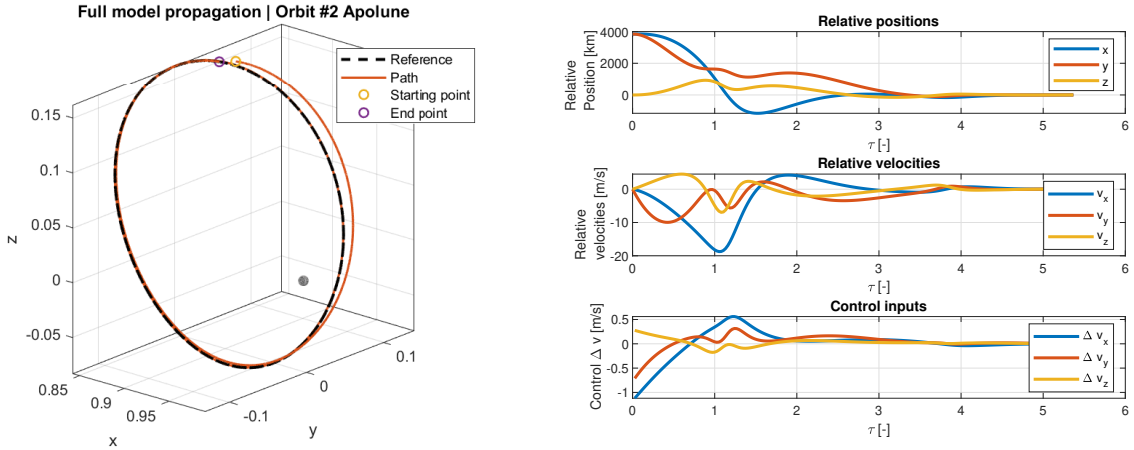

(a) Controlled trajectory **(b) State and control evolution**

Fig. 10 Simulation of the closed loop system for orbit #2 (apolune case).

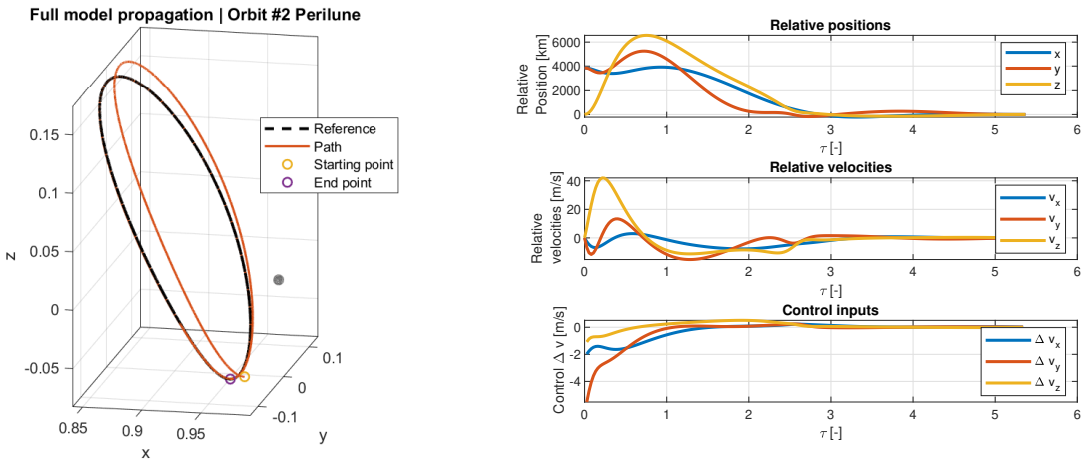

(a) Controlled trajectory **(b) State and control evolution**

Fig. 11 Simulation of the closed loop system for orbit #2 (perilune case).

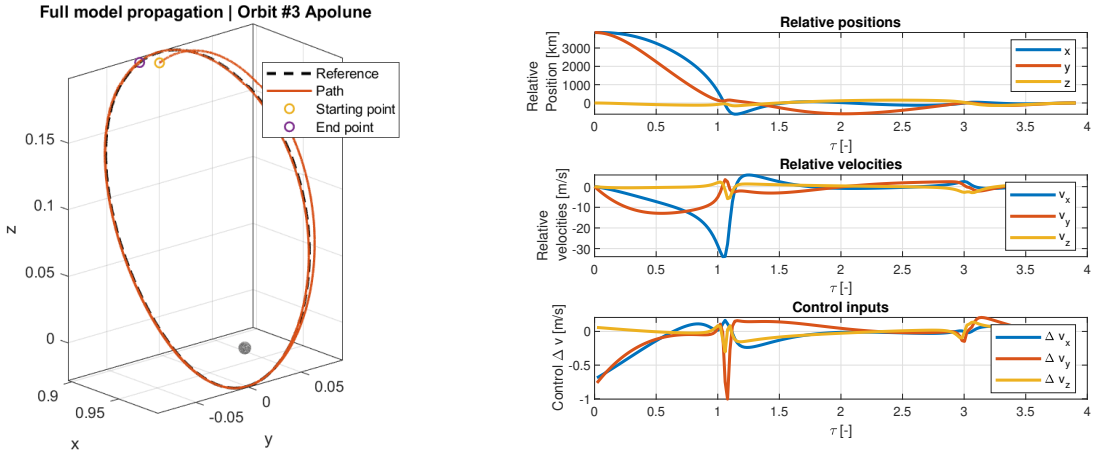

(a) Controlled trajectory **(b) State and control evolution**

Fig. 12 Simulation of the closed loop system for orbit #3 (apolune case).

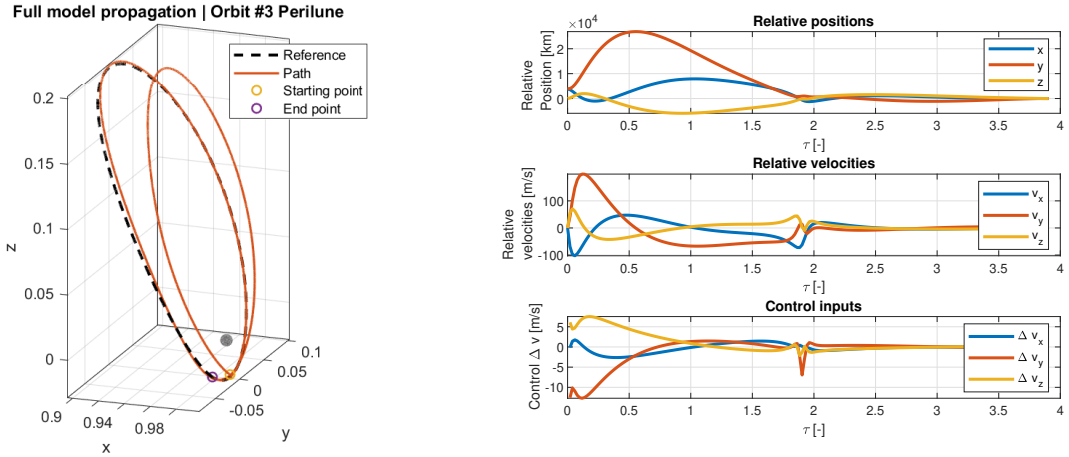

(a) Controlled trajectory **(b) State and control evolution**

Fig. 13 Simulation of the closed loop system for orbit #3 (perilune case).

The general trends for the total cost are maintained when varying the weight matrices. However, the values used are those that gave a balance between total cost and final error in the controller.

Table 4 Relative state of the chaser with respect to the target and control cost (in dimensional variables) after two full periods of simulation. Case refers to orbit number and perilune (P) or apolune (A).

Case	$\bar{x}(2T)[m]$	$\bar{y}(2T)[m]$	$\bar{z}(2T)[m]$	$\dot{\bar{x}}(2T)[m/s]$	$\dot{\bar{y}}(2T)[m/s]$	$\dot{\bar{z}}(2T)[m/s]$	$\Delta V[m/s]$
1A	9.094	-1.185	-20.715	1.571E-5	-6.399E-5	-1.593E-5	48.20
1P	203.416	-152.620	-22.802	3.219E-6	1.186E-4	4.103E-5	109.18
2A	16.869	-13.017	-29.495	-1.214E-5	-7.212E-5	1.221E-5	40.71
2 P	-21.136	39.402	112.014	1.069E-4	6.158E-4	-1.829E-4	119.06
3A	9.956	3.308	-17.745	3.234E-6	-3.402E-5	-8.254E-7	34.75
3P	-165.500	79.200	1338.701	2.881E-3	1.347E-2	-9.526E-3	482.09

6 Conclusions and future work

The described method allows us to compute a discrete-time LQR by using the Lyapunov-Floquet theory in periodic solutions of the CR3BP. This method greatly simplifies controller design and exhibits great performance both in terms of final error and control costs for the analyzed cases, compared with direct linearization and discretization of the CR3BP equations.

For future lines of work, an MPC controller design in line with [17, 18] will be proposed that takes the advantages that this change of variables offers. In this way, it would be possible to impose restrictions on the states and the control, modeling more accurately a real-world scenario.

Acknowledgments

R. Vazquez was supported by grant TED2021-132099B-C33 funded by MCIN/ AEI/ 10.13039 /501100011033 and by "European Union NextGenerationEU/PRTR."

J. Galan was supported by grant PID2021-123200NB-I00 of the Spanish Ministry of Science and Education.

References

[1] Mario Merri and Mehran Sarkarati. Lunar Orbiter Platform - Gateway: a clear use case for CCSDS MO services. In *2018 AIAA SPACE and Astronautics Forum and Exposition*, Orlando, Florida, United States of America, June 2018. DOI: https://doi.org/10.2514/6.2018-5337.

[2] Markus Landgraf, William Carey, Victoria Hipkin, James Carpenter, and Harald Hiesinger. HERACLES - exploring the moon in an international context. In *European Planetary Science Congress*, Berlin, Germany, September 2018.

[3] Ryan Whitley and Roland Martinez. Options for staging orbits in cislunar space. In *2016 IEEE Aerospace Conference*, Big Sky, Montana, United States of America, March 2016. DOI: https://doi.org/10.1109/AERO.2016.7500635.

[4] Emily M. Zimovan, Kathleen C. Howell, and Diane C. Davis. Near rectilinear halo orbits and their application in cis-lunar space. In *3rd IAA Conference on Dynamics and Control of Space Systems*, Moscow, Russia, May 2017.

[5] E. J. Doedel, R. C. Paffenroth, H. B. Keller, D. J. Dichmann, J. Galan-Vioque, and A. Vanderbauwhede. Computation of periodic solutions of conservative systems with application to the 3-body problem. *International Journal of Bifurcation and Chaos*, 13(6):1353–1381, 2003. DOI: https://doi.org/10.1142/S0218127403007291.

[6] G. Gomez, W. S. Koon, M. W. Lo, J. E. Marsden, J. Masdemont, and S. D. Ross. Connecting orbits and invariant manifolds in the spatial restricted three-body problem. *Nonlinearity*, 17(5):1571–1606, 2004. DOI: http://dx.doi.org/10.1088/0951-7715/17/5/002.

[7] Yuki Sato, Kenji Kitamura, and Takeya Shima. Spacecraft rendezvous utilizing invariant manifolds for a halo orbit. *Transactions of the Japan Society for Aeronautical and Space Sciences*, 58(5):261–269, 2015. DOI: https://doi.org/10.2322/tjsass.58.261.

[8] Haijun Peng, Chunfeng Yang, Yunpeng Li, Sheng Zhang, and Biaosong Cheng. Surrogate-based parameter optimization and optimal control for optimal trajectory of halo orbit rendezvous. *Aerospace Science and Technology*, 26(1):176–184, 2013. DOI: https://doi.org/10.1016/j.ast.2012.04.001.

[9] Giovanni Franzini and Mario Innocenti. Relative motion equations in the local-vertical local-horizontal frame for rendezvous in lunar orbits. In *2017 AAS/AIAA Astrodynamics Specialist Conference*, Stevenson, Washington, United States of America, August 2017.

[10] Wigbert Fehse. *Automated Rendezvous and Docking of Spacecraft*, pages 171–215. Cambridge University Press. Cambridge, UK, 1 edition, 2003. DOI: https://doi.org/10.1017/CBO9780511543388.

[11] Naomi Murakami, Satoshi Ueda, Toshinori Ikenaga, Maki Maeda, Toru Yamamoto, and Hitoshi Ikeda. Practical rendezvous scenario for transportation missions to cis-lunar station in Earth-Moon L2 halo orbit. In *25th International Symposium on Space Flight Dynamics (ISSFD)*, Munich, Germany, 2015.

[12] Brian L. Jones and Robert H. Bishop. Rendezvous targeting and navigation for a translunar halo orbit. *Journal of Guidance, Control and Dynamics*, 17(5):1109–1114, 1994. DOI: https://doi.org/10.2514/3.21317.

[13] Stephanie Lizy-Destrez, Laurent Beauregard, Emmanuel Blazquez, Antonino Campolo, Sara Manglativi, and Victor Quet. Rendezvous strategies in the vicinity of Earth-Moon Lagrangian points. *Frontiers in Astronomy and Space Sciences*, 5(45):1–19, 2019. DOI: https://doi.org/10.3389/fspas.2018.00045.

[14] Francisco Gavilan, Rafael Vazquez, and Eduardo Fernandez Camacho. Chance-constrained model predictive control for spacecraft rendezvous with disturbance estimation. *Control Engineering Practice*, 60:111–122, 2012. DOI: https://doi.org/10.1016/j.conengprac.2011.09.006.

[15] Cristophe Louembet, Denis Arzelier, and Georgia Deaconu. Robust rendezvous planning under maneuver execution errors. *Journal of Guidance, Control and Dynamics*, 38(1):76–93, 2015. DOI: https://doi.org/10.2514/1.G000391.

[16] M. Mammarella, E. Capello, H. Park, C. Guglieri, and M. Romano. Tube-based robust model predictive control for spacecraft proximity operations in the presence of persistent disturbance. *Aerospace Science and Technology*, 77:585–594, 2018. DOI: https://doi.org/10.1016/j.ast.2018.04.009.

[17] Julio C Sanchez, Francisco Gavilan, and Rafael Vazquez. Chance-constrained model predictive control for near rectilinear halo orbit spacecraft rendezvous. *Aerospace Science and Technology*, 100:105827, 2020. DOI: https://doi.org/10.1016/j.ast.2020.105827.

[18] Julio C. Sanchez, Francisco Gavilan, Rafael Vazquez, and Christophe Louembet. Spacecraft rendezvous hovering predictive control around a near-rectilinear halo orbit. In *Proceedings of the 2022 CEAS EuroGNC conference*. Berlin, Germany, 2022.

[19] Ethan R Burnett and Hanspeter Schaub. Spacecraft relative motion dynamics and control using fundamental modal solution constants. *Journal of Guidance, Control, and Dynamics*, 45(10):1786–1799, 2022. DOI: https://doi.org/10.2514/1.G006603.

[20] Eusebius J Doedel and B Oldeman. AUTO-07P: continuation and bifurcation software. *Montreal, QC: Concordia University Canada*, 1998.

[21] José Manuel Montilla García. AUTO-based numerical study of three body problem orbits and trajectories with applications to the lunar deep space gateway. *Masters' Thesis, ETSI, University of Seville*, 2018.

[22] Bernd Krauskopf, Hinke M Osinga, and Jorge Galán-Vioque. *Numerical continuation methods for dynamical systems*, volume 2. Springer, 2007.

[23] Pierre Montagnier, Christopher C Paige, and Raymond J Spiteri. Real Floquet factors of linear time-periodic systems. *Systems & control letters*, 50(4):251–262, 2003. DOI: https://doi.org/10.1016/S0167-6911(03)00158-0.

[24] Gerard Gómez, Josep Masdemont, and Carles Simó. Quasihalo orbits associated with libration points. *The Journal of the Astronautical Sciences*, 46:135–176, 1998. DOI: https://doi.org/10.1007/BF03546241.